J. Fluid Mech. (1975), *vol.* 70, *part* 1, *pp.* 161–177
Printed in Great Britain

Thermoacoustic effects in a resonance tube

By P. MERKLI AND H. THOMANN
Institute of Aerodynamics, Swiss Federal Institute of Technology, Zurich

(Received 10 September 1973 and in revised form 30 September 1974)

New experiments with a gas-filled resonance tube have shown that not only heating, but also cooling of the tube wall is possible and that these phenomena are not restricted to oscillation amplitudes that generate shocks. The present paper concentrates on amplitudes outside the shock region. For this case, an extended acoustic theory is worked out. The results show cooling in the section of the tube with maximum velocity amplitude (and thus dissipation) and marked heating in the region of the velocity nodes. A strong dependence of these effects on the Prandtl number is noted. The results are in good agreement with experiments. Although the theory is not valid for proper resonance conditions, it nevertheless sheds some light on what happens when nonlinear effects dominate.

Closely related to the limit of validity of the thermoacoustic theory is the question of transition from laminar to turbulent flow in the viscous boundary layer (Stokes layer). This problem has also been investigated; the results are given in a separate paper (Merkli & Thomann 1975). In the present article laminar flow is assumed.

1. Introduction

Sprenger (1954) published a paper describing his surprising experimental finding that the oscillating flow generated in a gas-filled tube by directing a jet into the open end (Hartmann–Sprenger tube) can produce strong heating of the closed end (temperatures of 1000 °K or more were observed). The attainable closed-end temperatures are much higher than the free-stream stagnation temperatures of the impinging jet. It was soon discovered that travelling shock waves are a main feature of the flow. Several authors (Sibulkin & Vrebalovich 1958; Hall & Berry 1959; Wilson & Resler 1959; Shapiro 1960) tried to explain the heating effect through the entropy increase due to these discontinuities. However, as the shock strength does not change along the tube, the heating does not change and these theories cannot explain why mainly the tube end is heated. Brocher & Maresca (1970, 1973) formulated a complete energy balance for the Hartmann–Sprenger tube and showed that wall friction can be a predominant mechanism for heat production. Moreover, they found that these tubes lose an appreciable amount of heat through mass exchange at the contact surface between the penetrating jet and the gas contained in the tube. This means that the approximately known boundary conditions at this contact surface are important for the full understanding of the flow in the tube. To overcome this

difficulty in our investigation, the tube length has been essentially doubled and the oscillations are now driven by small-amplitude harmonic oscillations of a flat piston in the vicinity of the velocity node, instead of by the 'gas piston' (jet) with large amplitude at the velocity antinode used to drive the Hartmann–Sprenger tube. With this arrangement, we always have the same gas in the tube and $u(x,R) = v(x,R) = u(L,r) = 0$, $u(0,r) = \hat{u}_0 e^{i\omega t}$ and $T(x,R) = T_0 = \text{constant}$, where u and v are the velocity components in the axial (x) and radial (r) directions respectively, T the temperature, t time, ω the radian piston frequency, L the tube length and R the tube radius.

The present paper (for full details see Merkli 1973) treats such a piston-driven resonance tube. Temperature measurements along the tube wall (§ 5) reveal the following.

(*a*) Heating of the closed end as in the Hartmann–Sprenger tube.

(*b*) Thermal effects that are also present outside the small frequency band around resonance where shock waves occur.

(*c*) Cooling of the tube wall (for shock-free motions) in the region of the velocity maximum, where dissipation is largest.

This paper focuses mainly on understanding the shock-free regime of oscillations. In this case, the acoustic theory can be applied by extending it to second order (thermoacoustic approach, § 2) to obtain an energy balance for the tube. The agreement between this theory and the experiments is good.

2. Theory

The basic equations governing the motion of a fluid are the axial and radial momentum equations, the continuity equation, the energy equation and the equation of state. For a perfect gas with constant specific heats c_p and c_v, constant dynamic viscosity μ and constant heat conductivity λ, these are (in cylindrical co-ordinates)

$$\rho\left[\frac{\partial u}{\partial t}+u\frac{\partial u}{\partial x}+v\frac{\partial u}{\partial r}\right] = -\frac{\partial p}{\partial x}+\mu\frac{1}{3}\frac{1}{r}\frac{\partial}{\partial r}\left(r\frac{\partial v}{\partial x}\right)+\mu\frac{4}{3}\frac{\partial^2 u}{\partial x^2}+\mu\frac{1}{r}\frac{\partial}{\partial r}\left(r\frac{\partial u}{\partial r}\right), \tag{1}$$

$$\rho\left[\frac{\partial v}{\partial t}+u\frac{\partial v}{\partial x}+v\frac{\partial v}{\partial r}\right] = -\frac{\partial p}{\partial r}+\mu\frac{4}{3}\left[\frac{1}{r}\frac{\partial}{\partial r}\left(r\frac{\partial v}{\partial r}\right)-\frac{v}{r^2}\right]+\mu\frac{1}{3}\frac{\partial^2 u}{\partial x\,\partial r}+\mu\frac{\partial^2 v}{\partial x^2}, \tag{2}$$

$$\frac{\partial \rho}{\partial t}+u\frac{\partial \rho}{\partial x}+v\frac{\partial \rho}{\partial r}+\rho\left[\frac{1}{r}\frac{\partial}{\partial r}(vr)+\frac{\partial u}{\partial x}\right] = 0, \tag{3}$$

$$\rho c_p\left[\frac{\partial T}{\partial t}+u\frac{\partial T}{\partial x}+v\frac{\partial T}{\partial r}\right] = \frac{\partial p}{\partial t}+v\frac{\partial p}{\partial r}+u\frac{\partial p}{\partial x}+\lambda\frac{1}{r}\frac{\partial}{\partial r}\left(r\frac{\partial T}{\partial r}\right)+\lambda\frac{\partial^2 T}{\partial x^2}$$
$$+\mu\frac{4}{3}\left[\left(\frac{\partial v}{\partial r}\right)^2+\left(\frac{\partial u}{\partial x}\right)^2+\left(\frac{v}{r}\right)^2-\frac{v}{r}\frac{\partial v}{\partial r}-\frac{\partial v}{\partial r}\frac{\partial u}{\partial x}-\frac{v}{r}\frac{\partial u}{\partial x}\right]+2\mu\frac{\partial v}{\partial x}\frac{\partial u}{\partial r}+\mu\left(\frac{\partial v}{\partial x}\right)^2+\mu\left(\frac{\partial u}{\partial r}\right)^2, \tag{4}$$

$$p = \rho R_g T, \tag{5}$$

where R_g is the gas constant, p the pressure and ρ the density.

In acoustics, where only small variations of the flow properties about a basic

state occur, a perturbation calculation can be used and the above equations simplified by setting (with $\epsilon \ll 1$)

$$\left.\begin{aligned} p &= p_0 + \epsilon p_1 + \epsilon^2 p_2 + \ldots, \\ T &= T_0 + \epsilon T_1 + \epsilon^2 T_2 + \ldots, \\ \rho &= \rho_0 + \epsilon \rho_1 + \epsilon^2 \rho_2 + \ldots, \\ u &= \quad \epsilon u_1 + \epsilon^2 u_2 + \ldots, \\ v &= \quad \epsilon v_1 + \epsilon^2 v_2 + \ldots . \end{aligned}\right\} \tag{6}$$

Terms of higher order are neglected. Note that $u_0 = 0$ as the basic state is at rest. In acoustics it is sufficient to consider terms up to first order in ϵ only. For the boundary conditions of a long tube ($L \gg R$) with uniform wall temperature T_0 (which allow further simplifications), the acoustic solution of the basic differential equations was given by Bergh & Tijdeman (1965):

$$p_1 = \left[-A \exp\left\{ \frac{\omega x}{a_0} \left(\frac{J_0(\alpha)}{J_2(\alpha)} \frac{\gamma}{n} \right)^{\frac{1}{2}} \right\} - B \exp\left\{ -\frac{\omega x}{a_0} \left(\frac{J_0(\alpha)}{J_2(\alpha)} \frac{\gamma}{n} \right)^{\frac{1}{2}} \right] e^{i\omega t}, \tag{7}$$

$$u_1 = \frac{-i}{\rho_0 a_0} \left(\frac{J_0(\alpha)}{J_2(\alpha)} \frac{\gamma}{n} \right)^{\frac{1}{2}} \left[A \exp\left\{ \frac{\omega x}{a_0} \left(\frac{J_0(\alpha)}{J_2(\alpha)} \frac{\gamma}{n} \right)^{\frac{1}{2}} \right\} - B \exp\left\{ -\frac{\omega x}{a_0} \left(\frac{J_0(\alpha)}{J_2(\alpha)} \frac{\gamma}{n} \right)^{\frac{1}{2}} \right\} \right] \times \left[1 - \frac{J_0(\alpha r/R)}{J_0(\alpha)} \right] e^{i\omega t}, \tag{8}$$

$$v_1 = \left[\frac{-i\omega}{\rho_0 a_0^2} \left(\frac{r}{2} \left\{ 1 - \frac{J_0(\alpha)}{J_2(\alpha)} \frac{\gamma}{n} \right\} + \frac{(\gamma-1) R}{\alpha Pr^{\frac{1}{2}}} \frac{J_1(\alpha r Pr^{\frac{1}{2}}/R)}{J_0(\alpha Pr^{\frac{1}{2}})} - \frac{\gamma}{n} \frac{R}{\alpha} \frac{J_1(\alpha r/R)}{J_2(\alpha)} \right) \right] p_1, \tag{9}$$

$$\rho_1 = \frac{1}{a_0^2} \left[1 + (\gamma - 1) \frac{J_0(\alpha r Pr^{\frac{1}{2}}/R)}{J_0(\alpha Pr^{\frac{1}{2}})} \right] p_1, \tag{10}$$

$$T_1 = \frac{1}{\rho_0 c_p} \left[1 - \frac{J_0(\alpha r Pr^{\frac{1}{2}}/R)}{J_0(\alpha Pr^{\frac{1}{2}})} \right] p_1, \tag{11}$$

where

$$\alpha \equiv R(\omega/\nu)^{\frac{1}{2}} e^{\frac{3}{4}\pi i}, \tag{12}$$

$$\frac{n}{\gamma} = \left(\gamma + (\gamma - 1) \frac{J_2(\alpha Pr^{\frac{1}{2}})}{J_0(\alpha Pr^{\frac{1}{2}})} \right)^{-1}, \tag{13}$$

γ is the ratio of the specific heats, a_0 the speed of sound and J_ν the Bessel function of the first kind of order ν. Fluid motion induced by harmonic oscillations of a flat piston is well described by this solution as long as the frequency is below the 'cut-off' frequency for radial oscillations and above the frequency where viscous nodes occur according to Scarton & Rouleau (1973). In this frequency range the pressure is uniform across the tube and, for high enough Reynolds numbers, a thin boundary layer (Stokes layer) forms at the wall. The present experiments are in this range.

The constants A and B are determined by the boundary conditions

$$u_1(x = 0) = \omega l e^{i\omega t} \quad \text{and} \quad u_1(L) = 0,$$

where l is the piston amplitude. The first condition cannot be satisfied exactly by (8), which is of the form $u_1 = f(x)\, g(r)\, e^{i\omega t}$. At present, the best way to resolve this difficulty seems to be to average u_1 over the cross-section at $x = 0$. For the

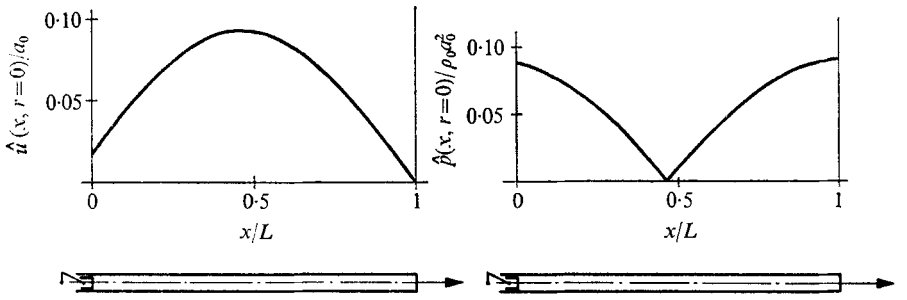

FIGURE 1. Amplitudes of axial velocity and pressure on the tube axis for the case $L = 1{\cdot}4$ m, $l = 13{\cdot}8$ mm, $R = 9{\cdot}5$ mm, $f = 115$ Hz, $f_{rs} = 122{\cdot}4$ Hz, air at $p_0 = 10^5$ N/m^2 and $T_0 = 298$ °K.

thin boundary layers of our experiments, the influence of the boundary layer may be neglected, leading to $u_1(x = 0, r = 0) = \omega l e^{i\omega t}$ and

$$A = i\rho_0 a_0 \omega l \left(\frac{J_2(\alpha)}{J_0(\alpha)}\frac{n}{\gamma}\right)^{\frac{1}{2}} \left[1 - \exp\left\{\frac{2\omega L}{a_0}\left(\frac{J_0(\alpha)}{J_2(\alpha)}\frac{\gamma}{n}\right)^{\frac{1}{2}}\right\}\right]^{-1},$$

$$B = A \exp\left\{\frac{2\omega L}{a_0}\left(\frac{J_0(\alpha)}{J_2(\alpha)}\frac{\gamma}{n}\right)^{\frac{1}{2}}\right\}.$$

Figure 1 gives typical distributions of the axial-velocity and pressure amplitudes along the tube axis according to (7) and (8).

The heating and cooling effects observed in the experiments are time averages. Therefore only terms of second (ϵ^2) and higher order in the energy equation contribute to them, and we have to extend the perturbation calculation of Bergh & Tijdeman to second order. For a boundary layer thin compared with R Burns (1967) gives solutions for the pressure up to order ϵ^4 for a progressive wave. Here we get for the second-order terms (with T_0 = constant)

$$\partial p_2/\partial r = 0, \tag{14}$$

$$\rho_0 \frac{\partial u_2}{\partial t} + \frac{\partial p_2}{\partial x} - \mu \frac{1}{r}\frac{\partial}{\partial r}\left(r\frac{\partial u_2}{\partial r}\right) = -\rho_0\left(u_1\frac{\partial u_1}{\partial x} + v_1\frac{\partial u_1}{\partial r}\right) - \rho_1\frac{\partial u_1}{\partial t}, \tag{15}$$

$$\frac{\partial \rho_2}{\partial t} + \rho_0\left[\frac{\partial v_2}{\partial r} + \frac{v_2}{r} + \frac{\partial u_2}{\partial x}\right] = -v_1\frac{\partial \rho_1}{\partial r} - u_1\frac{\partial \rho_1}{\partial x} - \rho_1\left[\frac{\partial v_1}{\partial r} + \frac{v_1}{r} + \frac{\partial u_1}{\partial x}\right], \tag{16}$$

$$\rho_0 c_p \frac{\partial T_2}{\partial t} - \frac{\partial p_2}{\partial t} - \frac{\lambda}{r}\frac{\partial}{\partial r}\left(r\frac{\partial T_2}{\partial r}\right) = -\rho_0 c_p\left[u_1\frac{\partial T_1}{\partial x} + v_1\frac{\partial T_1}{\partial r}\right] - \rho_1 c_p\frac{\partial T_1}{\partial t} + \mu\left(\frac{\partial u_1}{\partial r}\right)^2 + u_1\frac{\partial p_1}{\partial x}, \tag{17}$$

$$p_2 - \rho_0 R_g T_2 - \rho_2 R_g T_0 = \rho_1 R_g T_1. \tag{18}$$

The boundary conditions are $u_2 = v_2 = T_2 = 0$ at the tube wall.

These equations for the variables of second order (with subscript 2) correspond to those of Bergh & Tijdeman for the variables of first order if the right-hand sides are put equal to zero. Yet solution of the full second-order system involves much more labour than solution of the first-order one owing to the new inhomogeneous terms containing products of first-order variables. Fortunately it is not necessary

to solve the whole set if we are interested only in the local time-averaged heat flux penetrating into the tube wall, given by the relation

$$\langle q \rangle = \langle -\lambda [\partial T_2/\partial r]_R \rangle, \tag{19}$$

where angular brackets indicate time averages. In this case we can separate the energy equation (17) from the rest of the system (by time averaging) and integrate it independently with respect to r to yield the time average $\langle \partial T_2/\partial r \rangle$ of the temperature gradient at the tube wall. This procedure leads to the simple equation (see appendix)

$$\left\langle \frac{\partial T_2}{\partial r}\bigg|_R \right\rangle = \left\langle \frac{\rho_0 c_p}{\lambda R} \int_0^R r \frac{\partial (u_1 T_1)}{\partial x} dr \right\rangle. \tag{20}$$

As the quantities u_1 and T_1 are known [see (8) and (11)], the problem is reduced to an ordinary integration. It may readily be seen that the first-order variables can be represented, in complex notation, in the following manner:

$$u_1 = u_{1x}(x)\, u_{1r}(r)\, e^{i\omega t} \ldots, \quad \text{etc.}, \tag{21}$$

where $u_{1x}(x)$ and $u_{1r}(r)$ are the parts of u_1 depending on x and r alone respectively. With this notation and u_1^* as the complex conjugate of u_1, integration (20) yields the final result

$$\langle q \rangle = -\tfrac{1}{2} \mathrm{Re} \left\{ R\omega \left(\rho_0 u_{1x} u_{1x}^* + \frac{1}{\rho_0 a_0^2} \frac{J_0(\alpha)}{J_2(\alpha)} \frac{\gamma}{n} p_{1x} p_{1x}^* \right) \times \left(\frac{i}{2} - \frac{i\,Pr}{\alpha(1+Pr)} \frac{J_1(\alpha)}{J_0(\alpha)} - \frac{1}{\alpha\, Pr^{\frac{1}{2}}(1+Pr)} \frac{J_1^*(\alpha\, Pr^{\frac{1}{2}})}{J_0^*(\alpha\, Pr^{\frac{1}{2}})} \right) \right\}, \tag{22}$$

where Re denotes 'the real part of' and u_{1r} is defined by (8) as

$$u_{1r} \equiv [1 - J_0(\alpha r/R)/J_0(\alpha)]. \dagger \tag{23}$$

Numerical evaluation of equation (22) and those given by Bergh & Tijdeman [(7)–(11)] was carried out on a computer as high numerical accuracy is required, especially for cases near resonance.

† As pointed out by Rott (private communication), the final result (22) is still valid in the more general case where μ and λ are not assumed constant but are temperature dependent. With μ and λ expanded in power series (cf. pressure, temperature, etc.) the calculation follows the same lines as that given in this paper. The modification to the energy equation (17) is that the further term

$$-\frac{\lambda_1}{r} \frac{\partial}{\partial r} \left(r \frac{\partial T_1}{\partial r} \right)$$

appears on the left-hand side in addition to

$$-\frac{\lambda_0}{r} \frac{\partial}{\partial r} \left(r \frac{\partial T_2}{\partial r} \right).$$

But this term is part of $\langle q \rangle$ as (19) now becomes

$$\langle q \rangle = -\langle \lambda_0 [\partial T_2/\partial r]_R \rangle - \langle \lambda_1 [\partial T_1/\partial r]_R \rangle. \tag{19a}$$

Therefore the final result (22) is unaffected.

3. Discussion of the results

Equation (20) can be written in the form

$$2\pi R\langle q\rangle = -\frac{\partial}{\partial x}\left\langle 2\pi\rho_0 c_p \int_0^R r u_1 T_1 dr \right\rangle. \tag{20a}$$

As $c_p T_1 = h_1$, the first-order specific enthalpy, it states that an enthalpy flux

$$\langle E(x)\rangle = \left\langle 2\pi\rho_0 c_p \int_0^R r u_1 T_1 dr \right\rangle \tag{24}$$

exists in the tube. The variation of E with x corresponds to the heat exchanged with the tube wall.

Evaluation of (22) in the general case $\mu \neq 0$, $\lambda \neq 0$ shows that the energy introduced mechanically by the piston is not the only energy flowing into the tube. An additional amount of heat is absorbed from the environment in the region of the velocity maxima (at $x \approx \frac{1}{2}L$ in figure 1), though the heat production by dissipation is largest at the very same place. However, owing to the enthalpy flux $E(x)$, the dissipated mechanical energy and the heat absorbed in the region of the velocity maxima mainly show up at the velocity nodes – that is, at the closed end of the tube and at the piston.

In the ideal acoustic case ($\mu = 0$, $\lambda = 0$) no net energy flux exists in the tube as the phase difference between u_1 and p_1 (and thus T_1) in (24) equals $\frac{1}{2}\pi$. This means that the corrections arising from non-vanishing viscosity and heat conductivity (usually considered to be small) are the real and only 'sources' of the thermal effects arising from acoustic oscillations.

An interesting result is the strong dependence of the thermal effects on the Prandtl number Pr, illustrated in figure 2, which shows the behaviour of $q(x)$ for a tube with $L = 1{\cdot}4$ m. The Prandtl number, which for all gases is fairly close to 1, has in this example been altered artificially by variation of λ. The trend shown in figure 2 has been verified experimentally for $0{\cdot}5 < Pr < 0{\cdot}71$ (Merkli 1973). This is possible as gas mixtures have Prandtl numbers considerably smaller than those of the pure components, e.g. for air–helium mixtures Eckert, Ibele & Irvine (1960) measured $Pr_{\min} = 0{\cdot}45$ and for air–argon we calculated $Pr_{\min} = 0{\cdot}38$. From figure 2 we see the following.

(i) For $Pr \gg 1$, the energy flux in the tube becomes unimportant and the heat produced by dissipation appears near the velocity antinodes, where it is generated as predicted by 'naive' theories.

(ii) For $Pr = 1$, the cooling effect vanishes. Thus for the prediction of cooling effects, it is a bad approximation to set $Pr_{\text{air}} \approx 1$.

(iii) The smaller the Prandtl number the bigger the thermal effects (heating and cooling).

It is difficult to understand the details of the second-order energy flux, as it is generated by a combination of amplitude changes due to viscosity and heat conductivity and, much more important, by phase shifts between the quantities u_1, p_1, T_1, etc.: the phase differences are no longer equal to 0 or $\frac{1}{2}\pi$ as for $\mu = 0$, $\lambda = 0$, and in addition they depend on x and r. However, in the limiting case

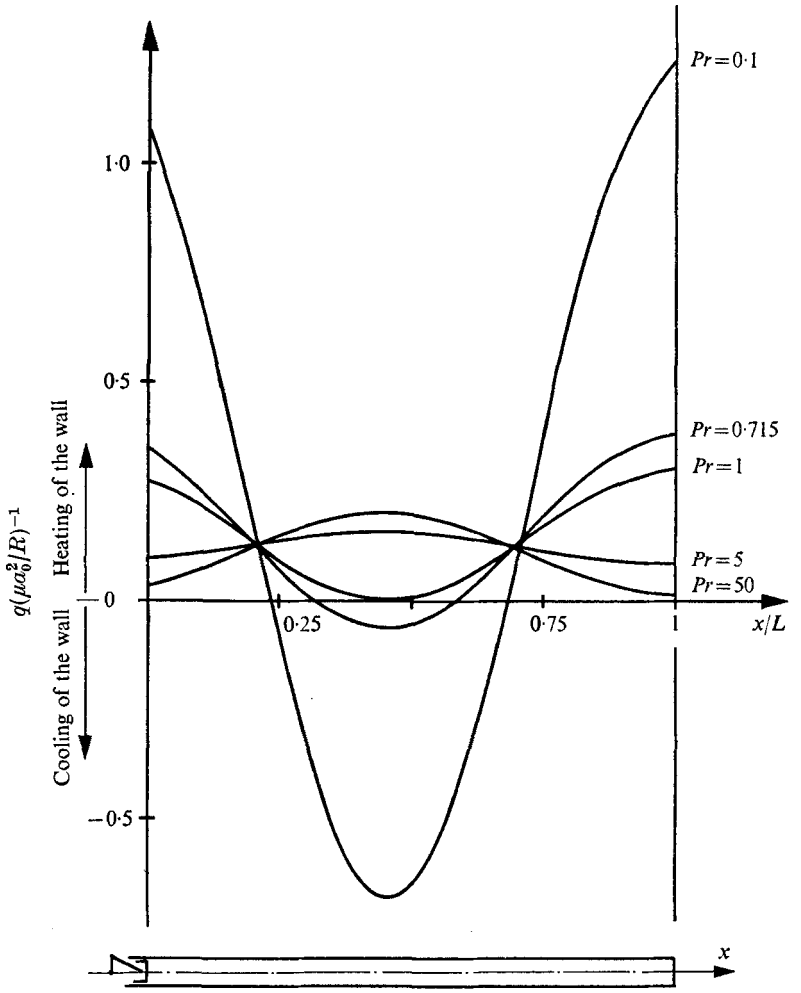

FIGURE 2. Thermal effects along the resonance tube for different Prandtl numbers (λ_{air} artificially altered in the calculations). $L = 1{\cdot}4\,\text{m}$, $l = 13{\cdot}8\,\text{mm}$, $R = 9{\cdot}5\,\text{mm}$, $f = 110\,\text{Hz}$, $f_{res} \approx 122\,\text{Hz}$, air at $p_0 = 10^5\,\text{N/m}^2$ and $T_0 = 298\,^\circ\text{K}$.

$|\alpha|^{-1} \equiv (\nu/\omega R^2)^{\frac{1}{2}} \to 0$, $Pr\,|\alpha|^2 \equiv \omega R^2 \rho_0 c_p/\lambda \ll 1$ the energy transport is easily demonstrated. Introducing α and $Pr^{\frac{1}{2}}\alpha$ into the expressions for p_1, u_1 and T_1 [see (7), (8) and (11)] and retaining only the leading terms, the results for a tube with a closed end at $x = L$ become

$$u_1 = \hat{u} \sin\left[\omega(L-x)/a_T\right] e^{i\omega t}, \tag{25}$$

$$p_1 = -i\rho_0 a_T \hat{u} \cos\left[\omega(L-x)/a_T\right] e^{i\omega t}, \tag{26}$$

$$T_1 = \frac{\rho_0 a_T \hat{u} \omega R^2}{4\lambda} \cos\frac{\omega(L-x)}{a_T}\left[1 - \frac{r^2}{R^2}\right] e^{i\omega t}, \tag{27}$$

with $a_T^2 = p_0/\rho_0$, the isothermal speed of sound.

In this approximation (vanishing viscosity, large conductivity, $Pr \to 0$) the thin velocity boundary layer makes a negligible contribution to the energy equation. It can therefore be discarded in (25), which reduces to the inviscid case. Owing to the high conductivity, the thermal boundary layer fills the whole tube cross-section and the radial temperature distribution becomes parabolic. Yet much more important is the phase difference between p_1 and T_1, as will be shown below. Inspection of the first-order energy equation

$$\rho_0 c_p \frac{\partial T_1}{\partial t} - \frac{\partial p_1}{\partial t} = \frac{\lambda}{r} \frac{\partial}{\partial r} \left(r \frac{\partial T_1}{\partial r} \right) \tag{28}$$

shows the reason for the change of phase. The ratio of the first term on the left side to the term on the right side is of order $Pr\,|\alpha|^2$. Without heat conduction, the term on the right side vanishes, leaving p_1 and T_1 in phase. With strong conduction, on the other hand, $Pr\,|\alpha|^2 \ll 1$ and the first term on the left side becomes negligible, leading to $T_1 \sim \partial p_1/\partial t$ and a phase difference of $\frac{1}{2}\pi$ between p_1 and T_1. Thus u_1 and T_1 [see (25) and (27)] are now in phase. A flow directed from the velocity maxima towards the nodes (that is, from the middle of the tube towards the piston and the tube end in the experiment) has a temperature above T_0 while a flow away from the nodes is below T_0. This leads to a net enthalpy flux $\langle E(x) \rangle$ towards the velocity nodes which is comparable to 'acoustic streaming'. As the dissipation is negligible, the enthalpy flux has to be compensated by heat exchanged with the tube wall. Combining (20), (25) and (27) we have

$$\langle q \rangle = Pr\,|\alpha|^2 \frac{\omega R \rho_0 \hat{u}^2}{32} \cos \frac{2\omega(L-x)}{a_T}, \tag{29}$$

which shows that the heating at the velocity nodes equals the cooling at the antinodes. The factor λ^{-1} ($Pr \sim \lambda^{-1}$) is not surprising as T_1 and thus the enthalpy flux vanish for very high conductivity.

In a recent paper Rott (1974) shows that the assumption of thin velocity and temperature boundary layers with $Pr \ll 1$ leads to $\langle q \rangle \sim Pr^{-\frac{1}{2}}$. An increase in λ will therefore first increase $\langle q \rangle$ until the thermal boundary layer fills the whole tube; a further increase in λ will decrease $\langle q \rangle$ again.

4. Experimental set-up and pressure measurements

Figure 3 shows the experimental arrangement. At one end of the tube, the oscillations are driven by a piston. In order to have simple and clear boundary conditions, it is essential that the piston performs a simple harmonic motion and therefore a special lag-free mechanical sine-motion generator was built which operates at frequencies $f = 0$–130 Hz and at piston amplitudes $l = 2{\cdot}85$–$13{\cdot}8$ mm. The other end of the tube is closed by a shiftable end piece so that different lengths may be set. This end piece contains a pressure transducer† which gives a reference signal, registered in every experiment. The pressure signal allows an exact determination of the oscillation frequency. To minimize vibrations of the

† Kistler charge amplifier, Type 566, with Kistler transducers, Type 410 A at the tube end and Type 412 along the tube.

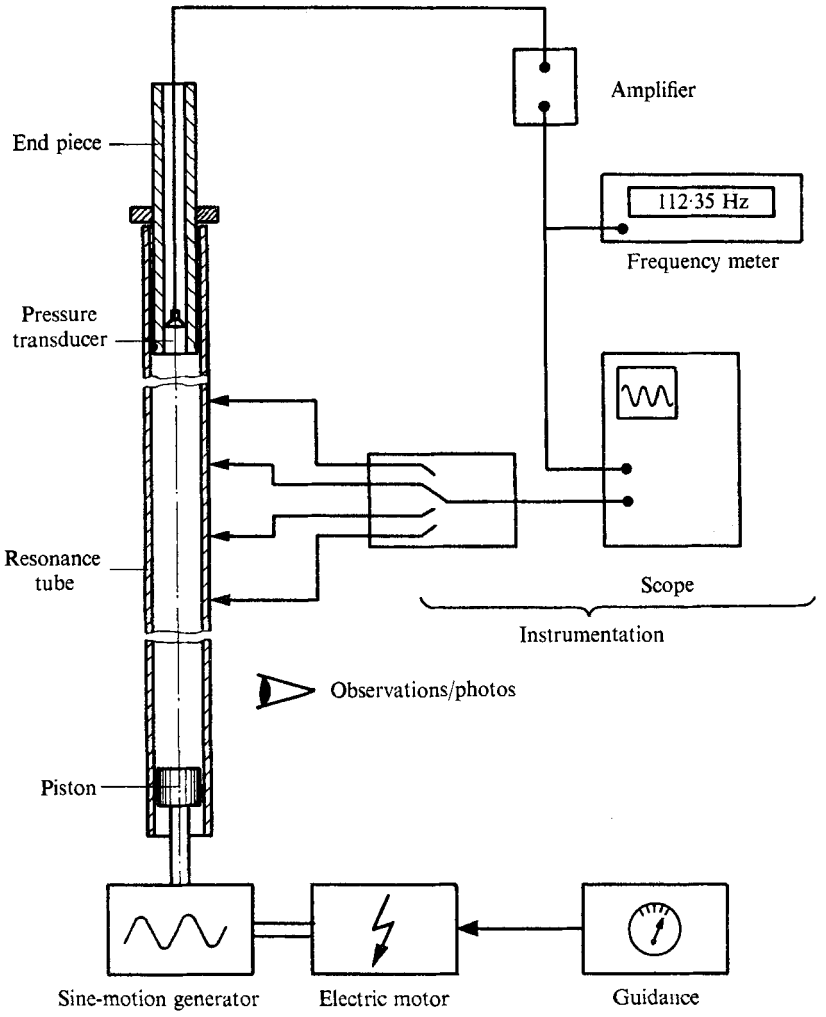

FIGURE 3. Experimental arrangement.

tube, the latter is connected by a short half-elastic section to the driving system. For different measurements along the tube (i.e. pressure, temperature), different tubes were used but these had mainly the same geometric parameters: $L = 1{\cdot}7$ m, $l = 13{\cdot}8$ mm, $R = 9{\cdot}5$ mm and $f_{\text{res}} \approx 100$ Hz. In the following such a tube will be referred to as the 'standard tube'.

First, different pressure measurements were made to examine the agreement between the real flow and the calculated one. Some results are plotted in figures 4–7. Figure 4 shows pressure measurements at the closed end of the standard tube for frequencies close to the resonance frequency of 100 Hz. We clearly see that, approaching resonance, the pressure signal is no longer a true sine wave (i.e. $f = 91{\cdot}6$ or $114{\cdot}7$ Hz) and that there exists a frequency band ($f = 93$–111 Hz) where shocks appear. This finding is in good agreement with the theoretical prediction of Chester (1964), especially if a correction to the resonance frequency

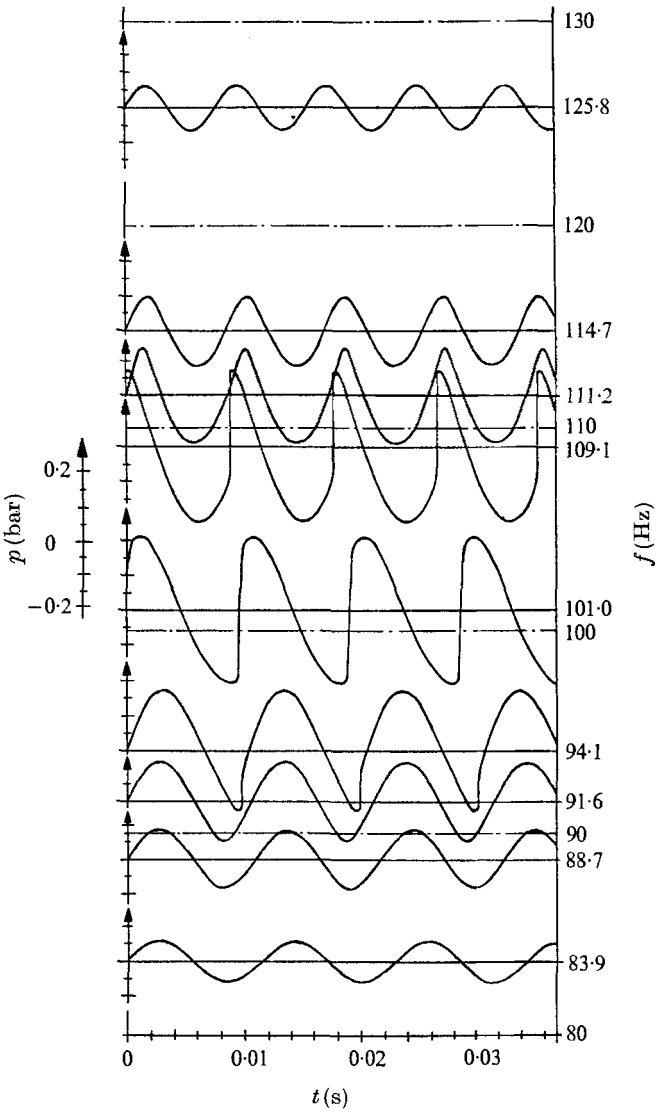

FIGURE 4. Pressure measurements at the closed end of the tube for frequencies around resonance. Standard tube, $L = 1{\cdot}7$ m, $l = 13{\cdot}8$ mm, $R = 9{\cdot}5$ mm, $f_{res} \approx 100$ Hz, air.

for non-vanishing μ is introduced (Merkli 1973). The real problem here is to find the speed of sound a_0 or the ambient temperature T_0 in the tube, because rather strong thermal effects can arise for frequencies near resonance, as will be seen in § 5. This is also the reason why in figure 5 the measured pressure amplitudes (standard tube) compare favourably with theory below resonance yet show a large scatter above the shock region. This scatter reflects the integral thermal influence for different passages (quick or slow) through resonance. If a smaller piston amplitude is chosen, the amplitudes of the oscillations decrease, the thermal effects diminish (as $(l/L)^2$) and the measured values of $\hat{p}$ fit the theoretical curves more closely.

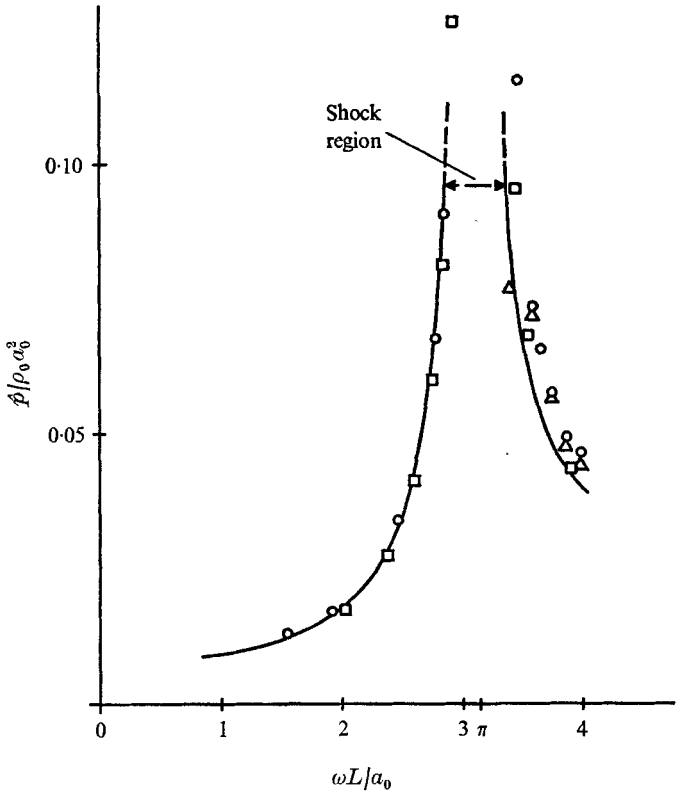

FIGURE 5. Pressure amplitudes at the closed end of the tube for different frequencies. Standard tube, $f_{res} \approx 100$ Hz. ——, theory of Bergh & Tijdeman (1965), air at $p_0 = 10^5$ N/m^2 and $T_0 = 298$ °K; ○, □, △, measurements.

From the experiments mentioned above we can say that, outside a frequency band slightly larger than the shock region, the agreement between measurements and the theory of Bergh & Tijdeman (1965) is excellent. The accuracy seems to be limited only by the uncertainty of the air temperature in the tube.

Figures 6 (*a*) and (*b*) show some further pressure measurements along the tube. Close to resonance ($f = 94{\cdot}1$ Hz or $\omega L/a_0 = 2{\cdot}92$) we see very well how shocks travel back and forth, whereas the curves for $f = 65{\cdot}4$ Hz or $\omega L/a_0 = 2{\cdot}03$ with sinusoidal time dependence confirm the theory of Bergh & Tijdeman.

5. Thermal measurements

In these experiments the heat capacity of the wall was used to measure the heat flux q by the transient technique. Full details are given by Merkli (1973). The resonance tube was mounted coaxially within a second, wider tube. In this manner an annular channel was formed, through which ambient air could be sucked in order to have a uniform temperature along the tube at the beginning of an experiment, and to insulate the tube with a layer of air at rest during the experiment itself. The wall thickness d and the tube material (a composite of

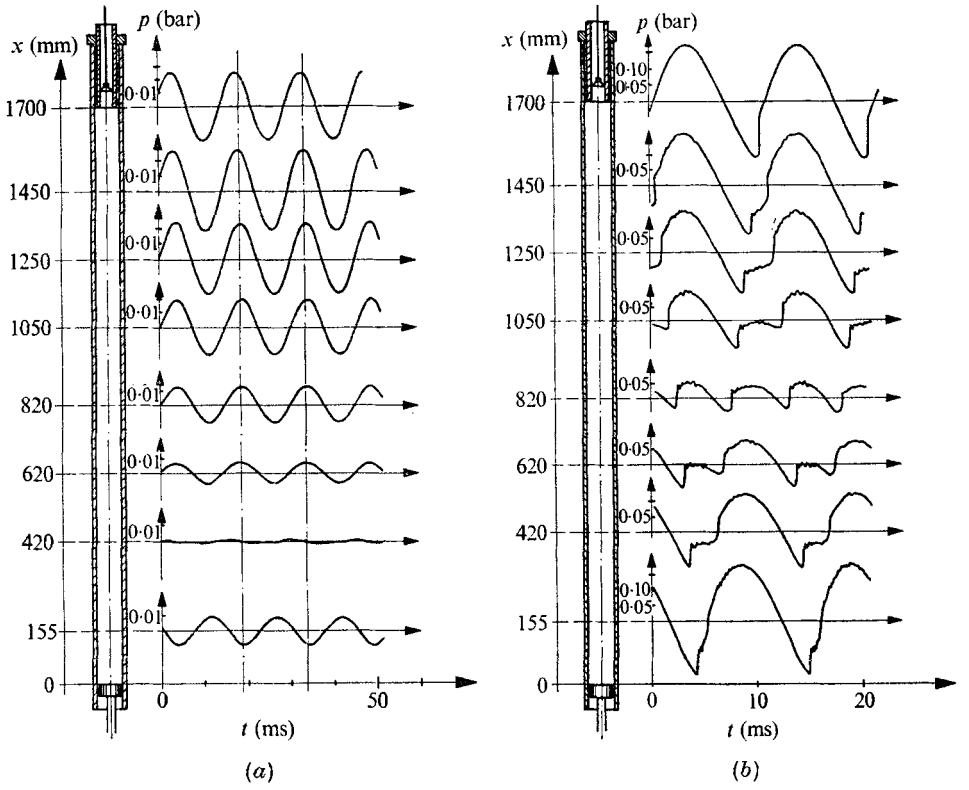

FIGURE 6. Pressure measurements along the tube. Standard tube, $f_{res} = 100$ Hz. (*a*) $f = 65{\cdot}4$ Hz. (*b*) $f = 94{\cdot}1$ Hz.

glass fibres and Araldite, determining the heat conductivity) were chosen such that axial heat conduction and radial temperature gradients could be neglected. Therefore, if an oscillation with a frequency near resonance was suddenly started, the heat produced by the oscillations began to heat the tube wall locally according to the relation

$$q = \rho c d(\partial T/\partial t) \tag{30}$$

and it was possible to determine $q(x)$ from temperature–time readings registered by thermocouples† built into the tube wall. The heat capacity ρcd of the tube was determined by calorimetry.

In figures 7–9 results of the thermal measurements for frequencies below, above and in the shock region are shown for the standard tube. We see the following.

(i) As predicted by the thermoacoustic theory, cooling occurs in the region of the velocity antinode if no shocks or, at the lower shock-region boundary, only weak shocks appear.

(ii) Thermal measurements compare favourably with the calculations as long as pressure measurements (§4) are in good agreement with theory (e.g. $\omega L/a_0 = 2{\cdot}59$ or $\omega L/a_0 = 2{\cdot}71$ in figure 7). This could be expected as no further assumptions had to be made for the thermal theory.

† Iron–constantan. Recorder: Honeywell, Lab/Test Recorder, Class 19.

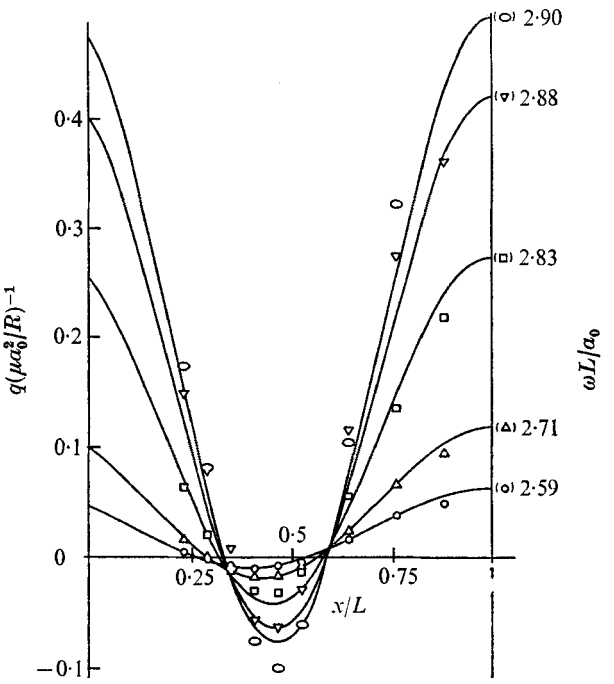

FIGURE 7. Thermal effects along the tube below resonance and shock conditions. Standard tube, air, $Pr = 0{\cdot}71$, $p_0 = 10^5\,\mathrm{N/m^2}$, $T_0 = 298\,^\circ\mathrm{K}$. ——, thermoacoustic theory (§ 2); ⬭, ▽, □, △, ○, measurements.

(iii) Towards the shock region slight departures of the measurements from the theory appear. This is not only due to the growing importance of nonlinearities but also to the appearance of turbulent bursts (see Merkli 1973; Merkli & Thomann 1975).

(iv) Above the shock region (figure 8) the agreement between experiment and theory is not as good as below. This finding has the same cause as the discrepancies found in the pressure measurements in the same region, namely that the passage through resonance with its strong thermal effects still has some lasting influence above resonance.

(v) At the lower boundary of the shock region (e.g. $\omega L/a_0 = 2{\cdot}90$, figure 7), the discrepancies between theory and experiment are smaller than at the upper boundary (e.g. $\omega L/a_0 = 3{\cdot}37$, figure 8).

(vi) The thermal effects are strongest in the shock region, with $q_{\max} = 300$–$400\,\mathrm{W/m^2}$ for the standard tube and $q_{\max} = 500\,\mathrm{W/m^2}$ for the case $L = 1{\cdot}4$ m, $l = 13{\cdot}8$ mm. As shown in figure 9 (or figure 4), the pressure amplitudes do not vary much in this frequency band. Likewise, the experimental curves for $q(x)$ are not very different from one another in contrast to those for frequencies outside the shock region. The cooling effect disappears here, yet the curves still have a minimum at the place predicted by the thermoacoustic calculations.

The work described thus far indicates the heat flux for a uniform wall temperature, but we still lack a feeling for the temperature differences it can produce.

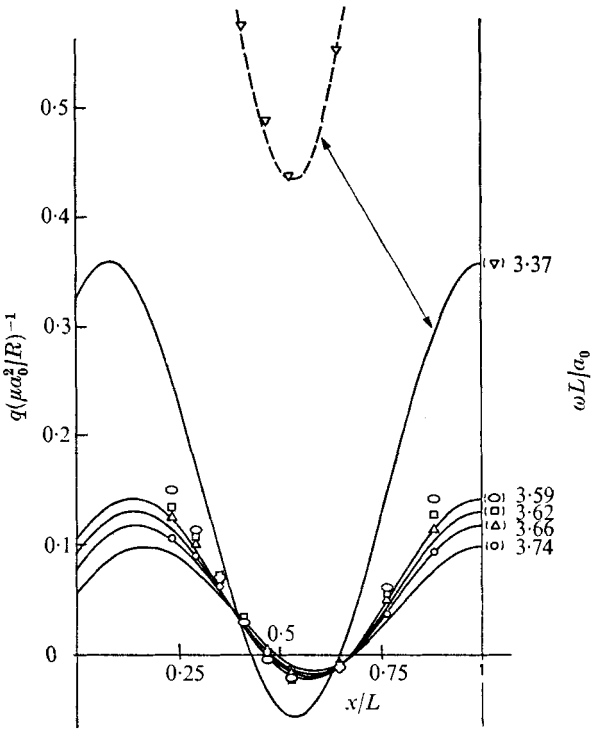

FIGURE 8. Thermal effects along the resonance tube above resonance and shock conditions. Standard tube, air, $Pr = 0{\cdot}71, p_0 = 10^5\,\mathrm{N/m^2}, T_0 = 298\,^\circ\mathrm{K}$. ——, thermoacoustic theory (§ 2); ⬭, ▽, □, △, ○, measurements.

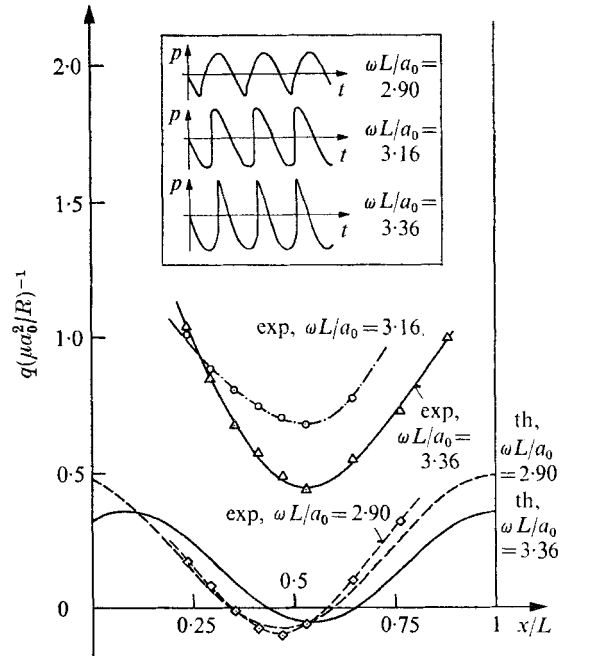

FIGURE 9. Thermal effects along the resonance tube in the shock region and corresponding pressure signals at the closed end of the tube. exp, experimental curves; th, curves according to the (here invalid) thermoacoustic theory.

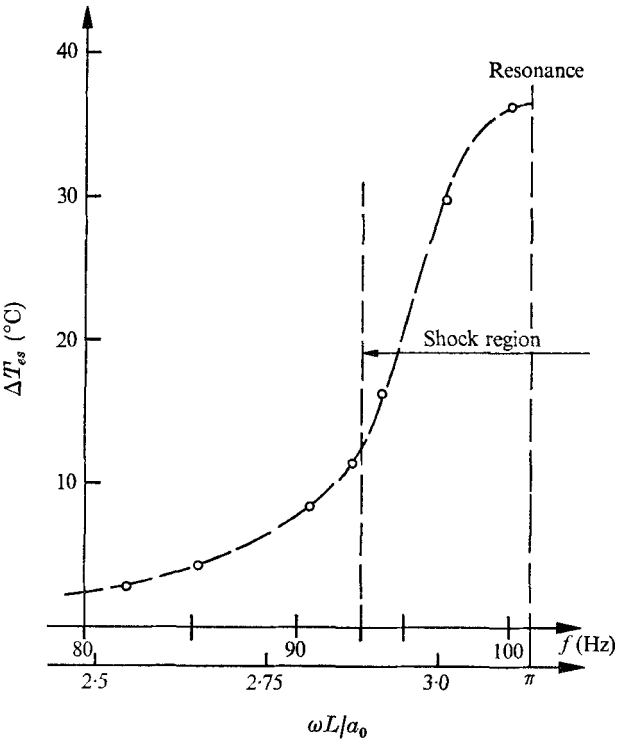

FIGURE 10. Steady temperature rises ΔT_{es} at the closed end for frequencies below resonance. Standard tube.

Figure 10 gives us some information on this effect. It shows the difference ΔT_{es} between the measured equilibrium temperature at the closed end of the standard tube and room temperature for frequencies below resonance. These values were reached after 15–20 min. They are the result of a balance between the heat generated in the tube and the ill-defined heat loss to the surroundings, still they give an indication of the temperature effects and of the mean temperature in the tube, as mentioned in § 4. The dependence of the steady temperature rise ΔT_s on x is similar to that of $q(\mu a_0^2/R)^{-1}$. However, as the piston continuously introduces mechanical energy into the well-insulated tube, no temperature decrease (except initially) was observed in the tube region near $x = \frac{1}{2}L$.

6. Conclusions and remarks

Some new results on the resonance tube were found. The most striking one is that cooling exists in the region of greatest dissipation due to friction. When shocks are absent, the new theory allows an accurate calculation of these effects. Discrepancies arise near resonance owing to nonlinearities and for strong oscillations also owing to turbulence. The occurrence of turbulence is treated in a separate paper (Merkli & Thomann 1975; or Merkli 1973). The present work is a further step towards an understanding of the Hartmann–Sprenger tube. Full

insight into the physical mechanisms in the shock region should be possible by an extension of Chester's (1964) theory. For strong oscillations, the influence of the turbulent bursts present in this case also has to be investigated.

Our treatment of the problem is limited to the calculation of the heat flux penetrating the tube wall. If we are interested in the details of the energy flux inside the tube, we have to solve the whole set of differential equations (14)–(18) for the second-order quantities, which is possible, but requires a lot of work.

In principle the resonance tube can be used as a heat pump. For this case, two questions remain unanswered.

(i) What temperature differences along the tube can be overcome by the heat flux? (In the present investigation the wall temperature was kept constant.)

(ii) What is the smallest Prandtl number that can be realized in gas mixtures (giving the maximum effectiveness of the device)?

The authors would like to acknowledge here interesting discussions with Professor Dr N. Rott and the valuable suggestions he made.

Appendix. Derivation of (20)

By substitution in the appropriate differential equations it can be verified that the quantities of second order have the forms

$$T_2 = T_{21}(x,r) + T_{22}(x,r)\,e^{2i\omega t}, \quad \text{etc.} \tag{A 1}$$

Therefore time averaging (17) gives

$$\left\langle \frac{\lambda}{r}\frac{\partial}{\partial r}\left(r\frac{\partial T_2}{\partial r}\right)\right\rangle = \left\langle c_p\rho_0\left(u_1\frac{\partial T_1}{\partial x}+v_1\frac{\partial T_1}{\partial r}\right)\right\rangle + \left\langle \rho_1 c_p\frac{\partial T_1}{\partial t}\right\rangle - \left\langle u_1\frac{\partial p_1}{\partial x}\right\rangle - \left\langle \mu\left(\frac{\partial u_1}{\partial r}\right)^2\right\rangle. \tag{A 2}$$

If this form of the energy equation is integrated over the tube cross-section the result is

$$\left\langle \lambda R\frac{\partial T_2}{\partial r}\bigg|_R\right\rangle = \left\langle c_p\rho_0\int_0^R r\left(u_1\frac{\partial T_1}{\partial x}+v_1\frac{\partial T_1}{\partial r}\right)dr\right\rangle + \left\langle c_p\int_0^R r\rho_1\frac{\partial T_1}{\partial t}\,dr\right\rangle - \left\langle \int_0^R r u_1\frac{\partial p_1}{\partial x}\,dr\right\rangle - \left\langle \mu\int_0^R r\left(\frac{\partial u_1}{\partial r}\right)^2 dr\right\rangle. \tag{A 3}$$

The continuity equation of first order,

$$\frac{\partial\rho_1}{\partial t}+\rho_0\left[\frac{\partial u_1}{\partial x}+\frac{1}{r}\frac{\partial(rv_1)}{\partial r}\right] = 0, \tag{A 4}$$

when multiplied by $c_p T_1$, time averaged and integrated over the tube cross-section becomes

$$\left\langle c_p\int_0^R rT_1\frac{\partial\rho_1}{\partial r}\,dr\right\rangle + \left\langle c_p\rho_0\int_0^R r\left(T_1\frac{\partial u_1}{\partial x}+\frac{T_1}{r}\frac{\partial(v_1 r)}{\partial r}\right)dr\right\rangle = 0. \tag{A 5}$$

This can easily be combined with the first two terms on the right-hand side of (A 3). The momentum equation of first order,

$$\rho_0\frac{\partial u_1}{\partial t}+\frac{\partial p_1}{\partial x}-\mu\frac{1}{r}\frac{\partial}{\partial r}\left(r\frac{\partial u_1}{\partial r}\right) = 0, \tag{A 6}$$

when multiplied by u_1, time averaged and integrated over the tube cross-section becomes

$$\left\langle \rho_0 \int_0^R r u_1 \frac{\partial u_1}{\partial t}\, dr \right\rangle + \left\langle \int_0^R r u_1 \frac{\partial p_1}{\partial x}\, dr \right\rangle - \left\langle \mu \int_0^R u_1 \frac{\partial}{\partial r}\left(r \frac{\partial u_1}{\partial r} \right) dr \right\rangle = 0. \quad \text{(A 7)}$$

Adding this to the last two terms of (A 3) gives

$$\left\langle \lambda R \frac{\partial T_2}{\partial r}\bigg|_R \right\rangle = \left\langle c_p \rho_0 \int_0^R r \frac{\partial (u_1 T_1)}{\partial x}\, dr \right\rangle + \left\langle c_p \rho_0 \int_0^R \frac{\partial (r v_1 T_1)}{\partial r}\, dr \right\rangle$$
$$+ \left\langle c_p \int_0^R r \frac{\partial (\rho_1 T_1)}{\partial t}\, dr \right\rangle + \left\langle \rho_0 \int_0^R r u_1 \frac{\partial u_1}{\partial t}\, dr \right\rangle - \left\langle \mu \int_0^R \frac{\partial}{\partial r}\left(r u_1 \frac{\partial u_1}{\partial r} \right) dr \right\rangle. \quad \text{(A 8)}$$

This is (20), $$\left\langle \frac{\partial T_2}{\partial r}\bigg|_R \right\rangle = \left\langle \frac{c_p \rho_0}{\lambda R} \int_0^R r \frac{\partial (u_1 T_1)}{\partial x}\, dr \right\rangle,$$

because all the other integrals in (A 8) vanish, those with partial derivatives with respect to r owing to the values at the integration limits and those with partial derivatives with respect to t owing to time averaging.

REFERENCES

Bergh, H. & Tijdeman, H. 1965 Theoretical and experimental results for the dynamic response of pressure measuring experiments. *Rep.* NLR-TR F. 238.

Brocher, E. & Maresca, C. 1970 Mécanisme des échanges thermiques dans un tube de résonance. *C. r. hebd. Séanc. Acad. Sci., Paris*, A **271**, 737.

Brocher, E. & Maresca, C. 1973 Etude des phenomènes thermiques dans un tube de Hartmann–Sprenger. *Int. J. Heat Mass Transfer*, **16**, 529.

Burns, S. H. 1967 Finite-amplitude distortion in air at high acoustic pressures. *J. Acoust. Soc. Am.* **41**, 1157.

Chester, W. 1964 Resonant oscillations in closed tubes. *J. Fluid Mech.* **18**, 44.

Eckert, E. R. G., Ibele, W. E. & Irvine, T. F. 1960 Prandtl number, thermal conductivity and viscosity for air–helium mixtures. *N.A.S.A. Tech. Note*, D-533.

Hall, J. M. & Berry, C. J. 1959 On the heating effect in a resonance tube. *J. Aero. Sci.* **26**, 253.

Merkli, P. 1973 Theoretische und experimentelle thermoakustische Untersuchungen am kolbengetriebenen Resonanzrohr. Dissertation, Eidgenössische Technische Hochschule, Zürich, no. 5151.

Merkli, P. & Thomann, H. 1975 Transition to turbulence in oscillating pipe flow. *J. Fluid Mech.* **68**, 567.

Rott, N. 1974 The heating effect connected with non-linear oscillations in a resonance tube. *Z. angew. Math. Phys.* **25**, 619.

Scarton, H. A. & Rouleau, W. T. 1973 Axisymmetric waves in compressible Newtonian liquids contained in rigid tubes: steady-periodic mode shapes and dispersion by the method of eigenvalleys. *J. Fluid Mech.* **58**, 595.

Shapiro, A. H. 1960 On the maximum attainable temperature in a resonance tube. *J. Aero Sci.* **27**, 66.

Sibulkin, M. & Vrebalovich, T. 1958 Some experiments with a resonance tube in a supersonic wind tunnel. *J. Aero. Sci.* **25**, 465.

Sprenger, H. 1954 Über thermische Effekte in Resonanzrohren. *Mitt. I.f.A.e., Eidgenössische Technische Hochschule, Zürich*, no. 21, p. 18.

Wilson, J. & Resler, E. 1959 A mechanism of resonance tube. *J. Aero. Sci.* **26**, 461.